Climate Dynamics (1998) 14:713–723

R.-H. Zhang · L. M. Rothstein

On the phase propagation and relationship of interannual variability in the tropical Pacific climate system

Received: 17 January 1997 / Accepted: 10 March 1998

Abstract—Upper ocean thermal data and surface marine observations are used to describe the three-dimensional, basinwide co-evolution of interannual variability in the tropical Pacific climate system. The phase propagation behavior differs greatly from atmosphere to ocean, and from equatorial to off-equatorial and from sea surface to subsurface depths in the ocean. Variations in surface zonal winds and sea surface temperatures (SSTs) exhibit a standing pattern without obvious zonal phase propagation. A nonequilibrium ocean response at subsurface depths is evident, characterized by coherent zonal and meridional propagating anomalies around the tropical North Pacific: eastward on the equator but westward off the equator. Depending on geographic location, there are clear phase relations among various anomaly fields. Surface zonal winds and SSTs in the equatorial region fluctuate approximately in-phase in time, but have phase differences in space. Along the equator, zonal mean thermocline depth (or heat content) anomalies are in nonequilibrium with the zonal wind stress forcing. Variations in SSTs are not in equilibrium either with subsurface thermocline changes in the central and western equatorial Pacific, with the former lagging the latter and displaced to the east. Due to its phase relations to SST and winds, the basinwide temperature anomaly evolution at thermocline depths on an interannual time scale may determine the slow physics of ENSO, and play a central role in initiating and terminating coupled air-sea interaction. This observed basinwide phase propagation of subsurface anomaly patterns can be understood partially as water discharge processes from the western Pacific to the east and further to high latitudes, and partially by the modified delayed oscillator physics.

R.-H. Zhang (✉) · L. M. Rothstein
Graduate School of Oceanography, University of Rhode Island, 215 South Ferry Rd., Narragansett, RI 02882, USA
E-mail: zrh@sequan.gso.uri.edu.

1 Introduction

The El Nino/Southern Oscillation (ENSO) phenomenon is the most prominent interannual variability in the tropical Pacific atmosphere-ocean system. One striking characteristic is a self-sustaining oscillation continually switching between a warm phase (El Nino) and a cold phase (La Nina). Such a continual oscillation implies the existence of both negative and positive feedback processes, and of anomaly propagation and phase lags between certain variables in the system. It is of central importance to determine what the phase propagation and lags are to explain and understand the physical mechanism responsible for the self-sustaining oscillation.

Bjerknes (1969) first proposed the basic air-sea coupling processes involving local positive feedbacks and phase differences between atmospheric and oceanic anomalies at the sea surface. In past decades, extensive observational analyses have illustrated certain key elements among the various atmosphere and ocean anomaly fields during an ENSO cycle, such as phase propagation and phase lag/lead relations (e.g., Wyrtki 1975, Rasmusson and Carpenter 1982). The possibility of low-frequency oscillations in the coupled system has been demonstrated in several *ad hoc* conceptual models (McWilliams and Gent 1978; McCreary and Anderson 1984). The corresponding unstable coupled modes can be identified in simplified tropical ocean-atmosphere systems (Philander et al. 1984; Yamagata 1985; Hirst 1986). Based on more realistic models, interannual variability corresponding to the observed ENSO phenomenon has been realized (e.g., Zebiak and Cane 1987; Schopf and Suarez 1988; Battisti and Hirst 1989; Zebiak 1989; and many others). General circulation model simulations have also reproduced ENSO-like phenomenon in more detail (e.g., Neelin 1990; Lau et al. 1992; Philander et al. 1992; Latif et al., 1993). Various oscillatory mechanisms have been proposed to

interpret simulated interannual variability, such as the delayed oscillator mode (Schopf and Suarez 1988; Battisti and Hirst 1989), the slow SST mode (Hirst 1986; Neelin 1990), and the recharge-discharge of equatorial heat content (Wyrtki 1986; Zebiak and Cane 1987; Zebiak 1989; Schneider et al. 1995).

Although current coupled models are able to simulate ENSO events realistically to some extent, there are significant intermodel differences (Neelin and Latif 1992; Philander et al. 1992). Detailed investigation of model tropical ocean-atmosphere interactions indicates that there are various types of coupled modes of relevance to interannual variability (e.g., Jin and Neelin 1993); several competing prototype models for ENSO have been proposed, with significant differences in phase propagation and relationship between anomalies in the ocean and atmosphere. One is a westward-propagating mode characterized by phase differences between equatorial SST and surface zonal winds (Hirst 1986; Neelin 1990). Another is known as the delayed oscillator mode, involving explicit equatorial wave propagation and reflection at the western boundary (Schopf and Suarez 1988; Battisti and Hirst 1989). Recent observations show a significant inconsistency between explicit single equatorial wave activity and El Nino evolution (e.g., Kessler and McPhaden 1995; Zhang and Levitus 1996, 1997). Philander et al. (1992), and Chao and Philander (1993) have further modified the delayed oscillator mechanism to explain their model interannual variability, interpreted as subsurface ocean phase propagation and its phase differences with SST. Indeed it has been demonstrated that subsurface ocean thermal anomalies behave very differently from those at the sea surface and may provide a possible memory mechanism responsible for the low-frequency oscillation in the coupled atmosphere-ocean system (e.g., White et al. 1989; Kessler 1990). Picaut et al. (1997) emphasize the important role of zonal displacement of the Pacific warm pool associated with advective processes and water-mass convergence in the oscillatory nature of ENSO. More recently, Jin (1996, 1997) presents a new conceptual recharge-discharge oscillator as a phase transition mechanism for ENSO, with nonequilibrium between zonal mean equatorial thermocline depth and wind stress, but without explicit zonal phase propagation. Observational analyses, including basin subsurface ocean thermal data, are necessary to determine which of the coupled modes is the most realistic. Based on decade-long observations, we will describe in this study subsurface phase propagation and its space-time relationship to some key anomaly fields.

2 Data and analysis procedures

The observed data include yearly atmospheric and oceanic anomalies in the tropical Pacific: surface zonal and meridional winds, sea level pressure (SLP), 20 °C isotherm depth, temperature at the upper ocean standard levels of sea surface, 10, 20, 30, 50, 75, 100, 125, 150, 200, 250, 300, and 400 m depths, and heat content (vertically averaged temperature anomalies in the upper 300 meter). The atmospheric variables are obtained from new analyses of surface marine anomalies which are derived from individual COADS observations from January 1945 to December 1989 (Da Silva et al. 1994). The oceanic data are based on the yearly *in situ* temperature anomaly fields analyzed by Levitus et al. (1994). In the present work, we prepare data sets on a 5° latitude-longitude grid by averaging the anomalies on a 1° latitude-longitude grid. The grid points are centered at 2.5 °N, 7.5 °N, 12.5 °N, etc., in latitude, and at 122.5 °E, 127.5 °E, 132.5 °E, etc., in longitude. The atmospheric anomalies are departures from the 1961–89 mean values and the oceanic anomalies are those from the 1961–90 mean values. In the eigenvalue problem, the observed data at a given grid point are actually anomaly data so that the elements of the matrix are covariance (Zhang and Levitus 1997).

Figure 1 shows variations in heat content, SST and surface zonal winds along the equator. There are structural and phase differences among these anomaly fields. Warm SST anomalies in the east are usually associated with westerly wind anomalies in the west. Both zonal wind and SST variations have a strong standing component centered respectively in the west and in the east. Heat content, on the other hand, shows a coherent phase propagation along the equator. Furthermore, there are clear phase relations both in time and in space between variations in SST, surface winds and heat content. This is further illustrated in Fig. 2, the regionally averaged anomalies on and off the equator. Surface zonal winds and SSTs along the equator fluctuate approximately in-phase in time, but have clear phase differences in space (Fig. 2a). Heat content anomalies in the west lead temporally SST variations in the east (or spatially showing westward displacements of the anomaly extremes). In particular, heat content anomalies appear to originate and intensify in magnitude in the western Pacific, and then propagate eastward along the equator. The time needed for the signals to move across the basin is about two years. Their arrival in the central and eastern equatorial Pacific results in a phase transition of SST anomalies, which in turn influences surface winds in the west, setting the stage for coupled air-sea interaction in the tropics. Thus, subsurface thermal anomalies can play an important role in initiating tropical Pacific air-sea interactions and ENSO cycling on interannual time scale. Furthermore, there are clear phase differences between heat content and winds along the equator (Fig. 2a), indicating that they are not in equilibrium. This suggests that the subsurface ocean has a memory of early wind forcing. Off the equator, heat content anomalies are approximately out-of-phase with surface wind stress curl (Fig. 2b).

To demonstrate coherent space-time variations in the tropical thermocline, Fig. 3 shows interannual fluctuations of the 20 °C isotherm depth on a circuit around the northern tropical Pacific. As is the case for heat content, the thermocline variability is also characterized by coherent phase propagation on and off the equator, and by phase differences in zonal structure from west to east. There is a hint of continual phase movement of anomaly patterns in succession, eastward along the equator (Fig. 3c), northward along the eastern boundary (Fig. 3d), westward off the equator of the tropical North Pacific (Fig. 3a), and equatorward along the western boundary (Fig. 3b). In some years associated with the El Nino and La Nina evolution, signals can be traced throughout such a complete circuit of the tropical North Pacific basin. This pattern can be explained as zonal and meridional exchanges of water mass from the western Pacific toward the east and further to higher latitudes during ENSO evolution (Wyrtki 1986; Zebiak 1989). This is further illustrated in Fig. 4a presenting variations in the 20 °C isotherm depth in the western and eastern equatorial Pacific and in the off-equatorial northeastern regions. The maximum and minimum thermocline depth anomalies are found at progressively later years along the equator from the west to east and to high latitude.

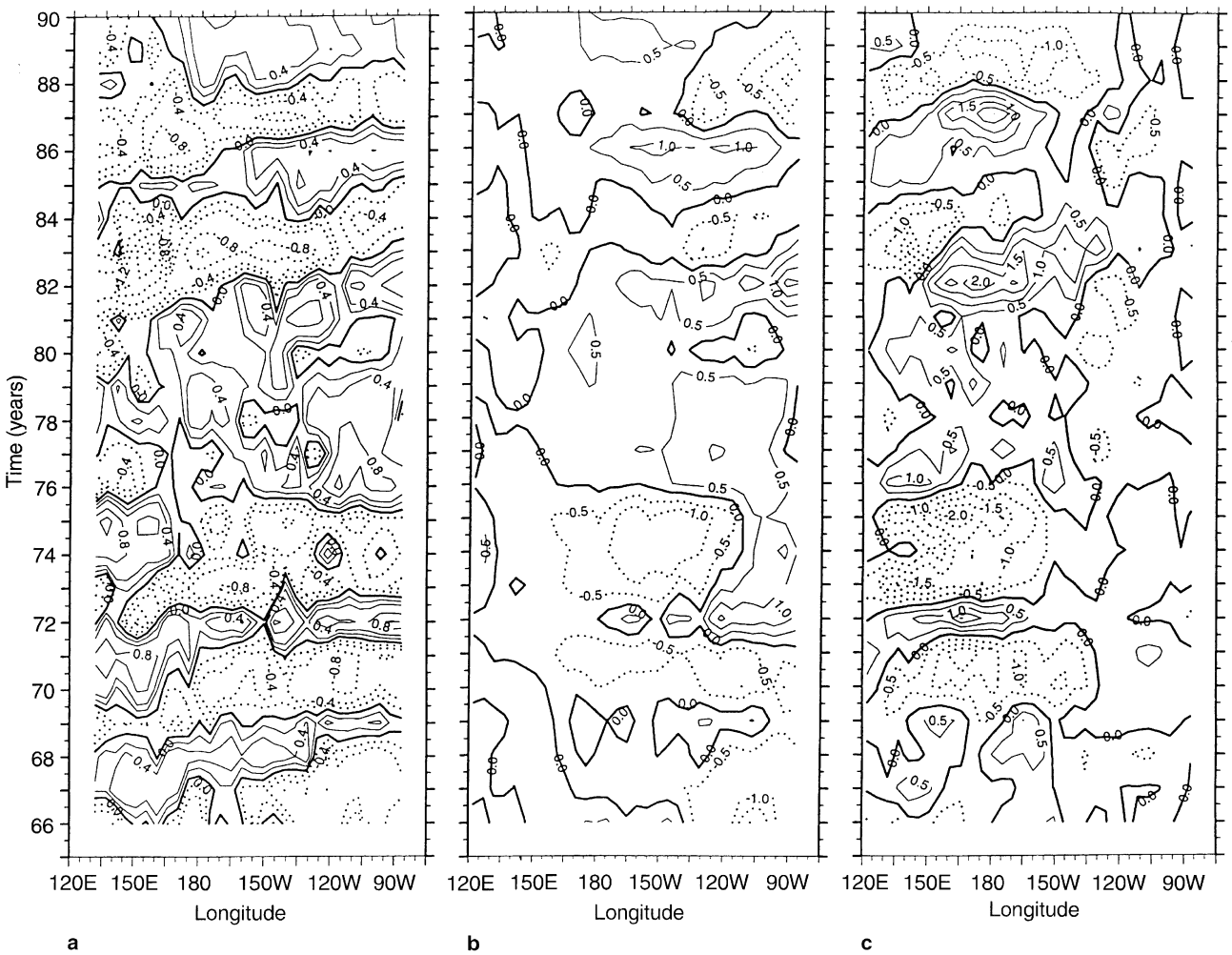

Fig. 1a–c Interannual variations in **a** heat content **b** SST and **c** surface zonal winds along the equator from 1966 to 1990. The contour interval is 0.2 °C in **a**, 0.5 °C in **b** and 0.5 m/s in **c**, with the *dotted line* being cold temperature anomalies in **a, b** and easterly wind anomalies in **c**

Finally, Fig. 4b shows zonal mean 20 °C isotherm depth anomalies along the equator and wind stress in the equatorial central Pacific. Zonal mean thermocline depth anomalies are not in equilibrium with zonal wind stress forcing along the equator. Before El Nino, there is a peak of positive thermocline depth anomaly (i.e., a depression of the thermocline); after El Nino, there is sharp shoaling of the thermocline along the entire equatorial Pacific, while there is a corresponding deepening off the equator (not shown). In addition, variations in SSTs are not in equilibrium either with the thermocline changes either (compare Fig. 2a with Fig. 4b).

3 Regression pattern

Zhang and Levitus (1997) have shown time variations of the first EOF mode for some atmospheric and oceanic variables. It is clearly evident from that study that different parameters in the coupled system vary coherently with time so that interannual fluctuations involve active interaction between the ocean and atmosphere. These relations can be investigated by computing linear regression between some reference time series and various anomaly fields.

Since the time variations of the first EOF mode for SLP and the spatial pattern represent the Southern Oscillation well, they are chosen as the reference time series upon which atmospheric and oceanic anomaly fields are linearly regressed. Following the analysis technique used by Lau et al. (1992), regression coefficients, referred to as regression pattern, can be calculated between gridpoint values and this reference time series at different time lags. We have performed this regression computation on atmospheric surface variables (SLP, zonal and meridional components of surface winds), and ocean thermal fields (the 20 °C isotherm depth, ocean temperature at the standard oceanographic analysis levels). Figures 5–8 show, with a one-year interval, the horizontal distributions of regression patterns for surface winds, SST and the 20 °C isotherm depth, and the zonal-depth sections of upper ocean temperature anomalies along the equator, thus

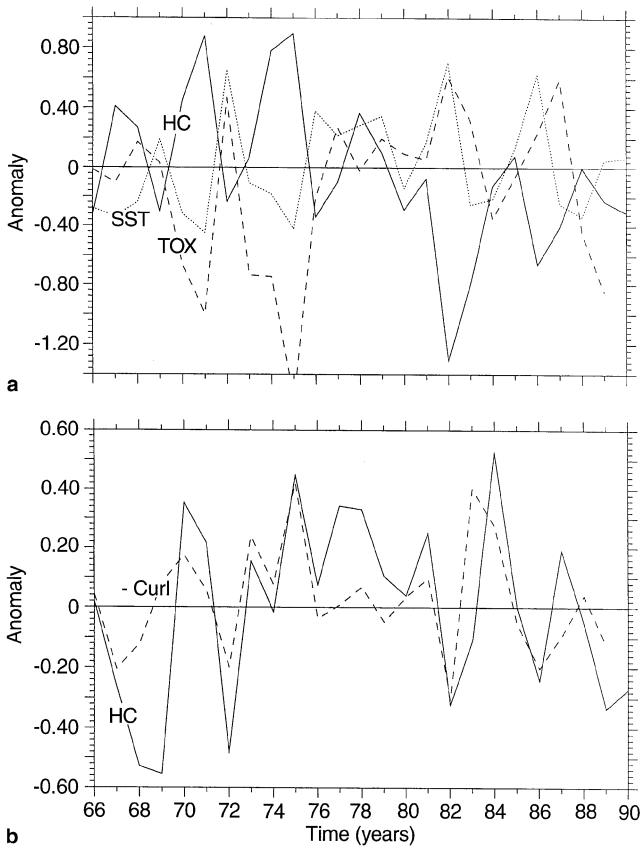

Fig. 2a Anomaly time series of heat content (*solid line*; scale unit: °C) averaged in regions (120 °E–160 °E, 2.5 °N–2.5 °S), zonal wind stress (*dashed line*; unit: N m^{-2}) averaged in regions (160 °E–160°W, 2.5 °N–2.5 °S), and of SST (*dotted line*; unit: °C) averaged in regions (160 °W–70°W, 2.5 °N–2.5 °S), respectively. Anomalies have been scaled by multiplying by 0.5 for SST and by 80 for wind stress. **b** Anomaly time series of heat content (*solid line*; scale unit: °C) averaged in regions (120 °E–160 °E, 12.5 °N–17.5 °N), minus wind stress curl (*dashed line*; unit: N m^{-3}) averaged in regions (160 °E–160 °W, 12.5 °N–17.5 °N), respectively. Anomaly has been scaled by multiplying by 0.8×10^8 for wind stress curl

providing a three-dimensional, basinwide picture of the space-time co-evolution. For example, since the positive amplitudes of the first SLP EOF mode coincide with positive anomalies in the western Pacific and negative anomalies to the east, the derived regression patterns at zero lag correspond to El Nino conditions (Fig. 7).

Figure 5 shows atmospheric and oceanic anomalies approximately two years before the warm phase, i.e., corresponding approximately to La Nina anomalies. Negative SST anomalies cover the eastern equatorial Pacific and South American coast regions, whereas positive SST anomalies are found in the central and western Pacific (Fig. 5b). Easterly wind anomalies are observed in the equatorial regions, accompanied by significant off-equatorward (divergent) wind anomalies over the eastern and central Pacific, i.e., an intensification of trade winds (Fig. 5a). Note that there is an enhanced anticyclonic surface circulation over the western tropical North Pacific near the date line (Fig. 5a). Correspondingly, the 20 °C isotherm depth anomalies are negative in the far eastern tropics but positive in the west, with maxima in the off-equatorial tropical North Pacific near the date line. The vertical displacement of the equatorial thermocline can be seen in the vertical-zonal section of temperature anomalies along the equator (Fig. 5d). A negative temperature anomaly is found in the eastern upper ocean, whereas there is a large positive anomaly at thermocline depths in the west.

One year prior to the warm phase (at lag –1 year; Fig. 6), the easterly wind anomalies become weaker in the central equatorial Pacific and westerly wind anomalies have developed in the tropics west of the date line. In the South Pacific, surface winds show a general pattern of westerly to northwesterly anomalous flow across most of the Pacific south of 10 °S, reflecting a diminution of the southeast trade winds. From lag –2 years to lag –1 year, the subsurface temperature anomalies in the west appear to propagate along the equator; cold conditions decay in the east. There are positive temperature anomalies in the central and eastern upper ocean but negative anomalies in the far western Pacific. As a result, the positive SST anomalies disappear west of the date line but develop to the east.

During the warm phase near zero lag (Fig. 7), warm conditions prevail in the tropical Pacific. The positive subsurface temperature anomaly has propagated across the equatorial basin. The structure of thermocline displacement is strikingly different in the west and in the east. Subsurface temperature anomalies in the west have opposite sign to those in the east. Large positive SST anomalies now cover a huge region of the central and eastern Pacific Ocean. Correspondingly, westerly anomalies have strengthened and spread eastward to prevail over a vast area of the western and central equatorial Pacific, accompanied by an anomalous equatorward flow in both hemispheres. In addition, there is an anomalous northerly flow across the normal position of the ITCZ in the tropical North Pacific, reflecting its southward shift.

One year after the warm phase (Fig. 8), cold waters, which appear first at subsurface depths in the west (Fig. 7d), have expanded and propagated eastward across the equatorial basin (Fig. 8d). Their arrival in the east results in a cooling in the eastern equatorial upper ocean. A striking feature is an opposite temperature changes on, and north of the equator. The thermocline shoals in the entire equatorial region whereas it deepens off the equator to the north (Fig. 8c). Negative SST anomalies reappear in the eastern equatorial Pacific and along the South and central American coasts (Fig. 8b). Easterly wind anomalies are located west of the date line, with an anomalous anticyclonic flow in the northwestern Pacific regions (Fig. 8a). There

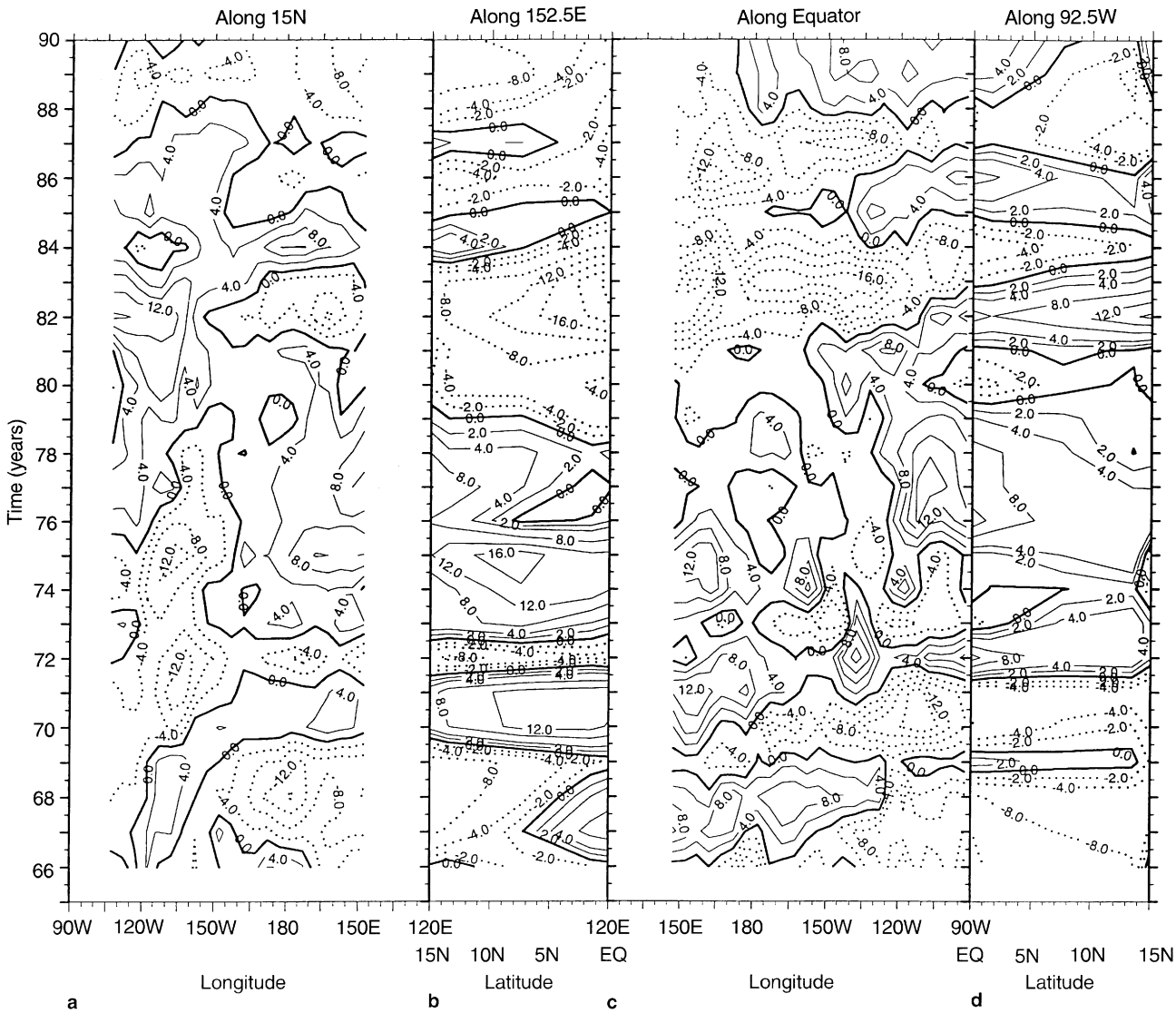

Fig. 3a–d Interannual variations in the 20 °C isotherm depth on a circuit around the northern tropical Pacific. **a** Zonal section along 15 °N; **b** meridional section along 152.5 °E; **c** zonal section along the equator; **d** meridional section along 92.5 °W. *Note* the *east* to *west reversal* in *plotting* the *longitude* for the two zonal sections **a, c** and the *north* to *south reversal* in plotting the *latitude* for the two meridional sections **b, d** in order to emphasize better a continuous circuit at their intersections. The contour interval is 4 m in **a** and **c**, and is 2 m in **b** and **d**, respectively. The *solid* and *dotted lines* indicate respectively deepening and shoaling of the thermocline

are enhanced southwest trade winds over the South Pacific Ocean. Two years after the warm phase, La Nina reappears. The spatial patterns are similar to those at lag –2 (Fig. 5).

Figure 9 shows the zonal-depth sections of the regression patterns for upper ocean temperature anomalies along 12.5 °N at lag 0 and lag +1 years, respectively. There are coherent variations in ocean temperature on and off the equator, with a phase connection between anomaly patterns in the eastern boundary regions. During an El Nino year, anomalies are negative in the west but positive in the east on the equator (Fig. 7d). One year after El Nino, the positive anomaly has moved into the off-equatorial North Pacific (Fig. 9b). We can see a striking phase contrast of upper ocean temperature anomalies on and off the equator (Figs. 8d and 9b). Further, the off-equatorial positive anomaly from the equator appears to propagate westward from the eastern boundary. Since westerly wind anomalies associated with the previous El Nino (Fig. 7a) would lift the off-equatorial thermocline in the central and western Pacific and correspondingly result in *cold* subsurface temperature anomalies off the equator (e.g., Chao and Philander 1993), the observed *warm* anomalies in the central and western Pacific (Fig. 9b) should be considered as a continually propagating signal from the east (Fig. 9a). From lag 0 year (Fig. 9a) through lag +1 year

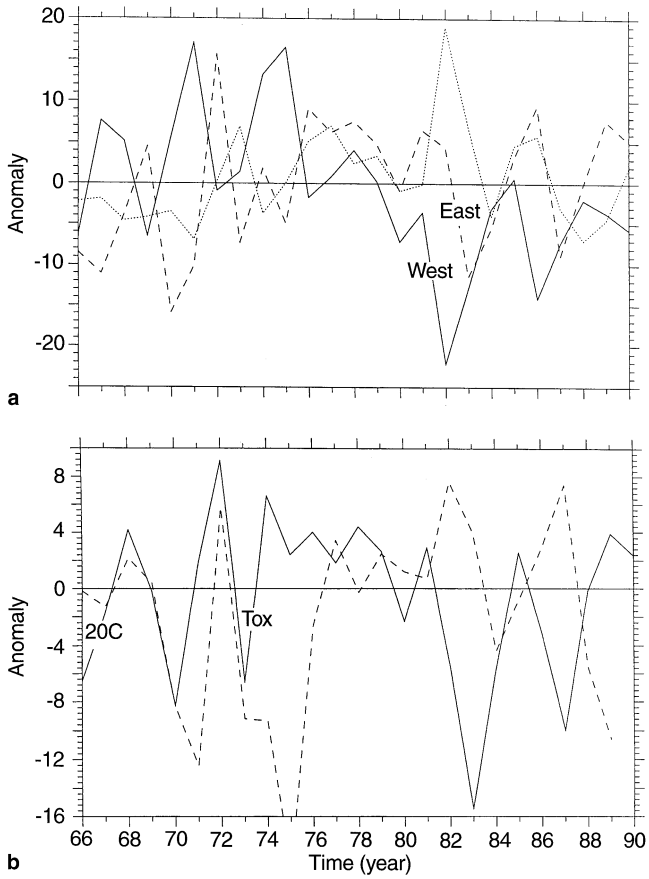

Fig. 4 a Anomaly time series of 20 °C isotherm depth (scale unit: m) averaged in regions (120 °E–160 °E, 2.5 °N–2.5 °S) (*solid line*), (140 °W–70 °W, 2.5 °N–2.5 °S) (*dashed line*), and (120 °W–70 °W, 12.5 °N–17.5 °N) (*dotted line*), respectively. **b** Anomaly time series of zonal mean 20 °C isotherm depth (scale unit: m) along the equator (*solid line*), and zonal wind stress (*dashed line*) averaged in the central equatorial Pacific regions (160 °E–160 °W, 2.5 °N–2.5 °S), respectively. The anomaly has been scaled by multiplying by 10^3 for wind stress

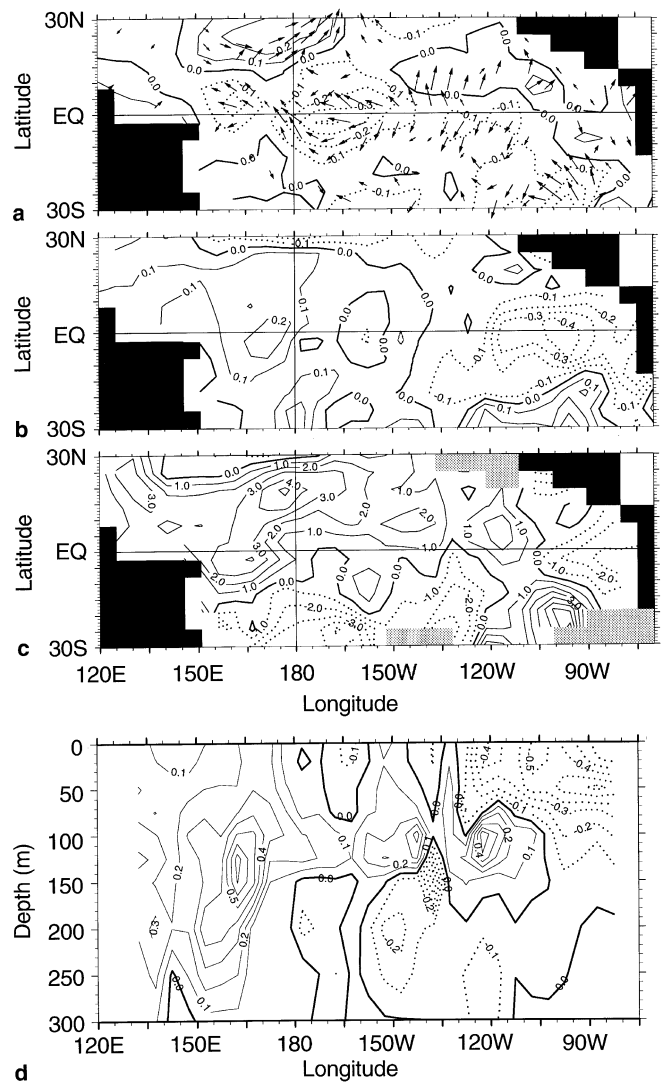

Fig. 5a–d The linear regression patterns of horizontal distribution with the reference time lagging the gridpoint data by two years for **a** surface winds (*arrow*) and the zonal component (contour; interval: 0.1 m s^{-1}), **b** SST (interval: 0.1 °C) and **c** the 20 °C isotherm depth (interval: 1 m), and **d** zonal-depth section for upper ocean temperatures along the equator (interval: 0.1 °C), respectively

(Fig. 9b), the off-equatorial positive anomaly has indeed propagated westward across the basin to the west and will continue to move toward the equator in the western boundary regions and may serve as the origin of the next warm event as demonstrated in Fig. 3b. This interesting feature of observed El Nino evolution has not been reasonably simulated in previous modeling studies.

4 Phase propagation

To present the phase propagation behavior of atmospheric and oceanic anomalies more clearly, we display longitude-time lag distributions of the regression coefficients for various anomalies on and off the equator. This can show that the phase propagation differs greatly from atmosphere to ocean, and from on the equator to off the equator and from sea surface to subsurface depths in the ocean. Variations in surface zonal winds do not show distinct phase propagation but are largely dominated by a standing pattern. Similarly, SST changes also exhibit a standing component with the largest variability in the central and eastern equatorial Pacific.

The space-time variations in temperature at, for example, 125 m depth tell quite a different story. Although equatorial SST anomalies are small in the west, subsurface temperature anomalies are significantly large in the western Pacific, and possess a consistent pattern which is opposite in phase to those in the eastern equatorial Pacific. Unlike variations in surface zonal winds and SST, subsurface temperature anomalies show coherent phase propagation both on

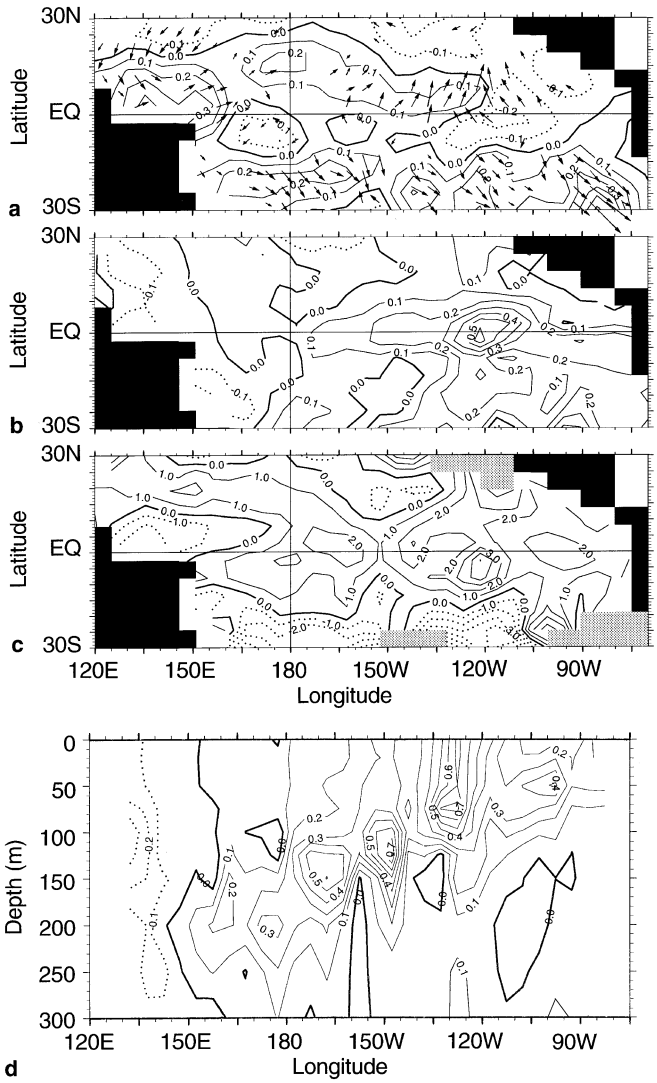

Fig. 6a–d The same as in Fig. 5 but for the reference time lagging gridpoint data by one year

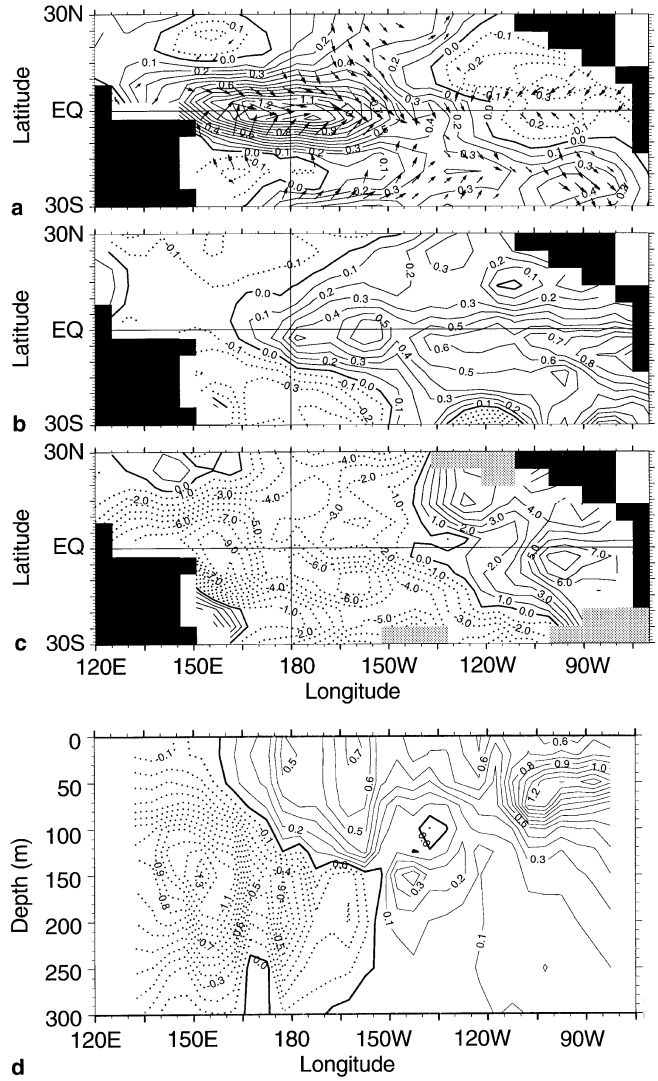

Fig. 7a–d The same as in Fig. 5 but for the reference time in phase with the gridpoint data

and off the equator. Figure 10 presents the 20 °C isotherm depth anomalies in time-longitude and time-latitude sections consisting of the equatorial wave guide, off-equatorial tropical North Pacific, and tropical eastern and western boundary regions. As demonstrated in Fig. 3, the anomalies appear as a continuous band running from west to east on the equator (Fig. 10c) and then from east to west off the equator (Fig. 10a), with apparent phase continuity in the western (Fig. 10b) and eastern (Fig. 10d) Pacific regions.

5 Phase relationships

Figures 11–12 display the amplitude of the regression coefficients in two typical equatorial regions. The data fields displayed here include SLP, SST, zonal wind component, the 20 °C isotherm depth, and ocean temperatures at 50 m and 125 m depths, respectively. Some of these values have been multiplied by a time-invariant factor so that they can be easily discerned. Note that when interpreting the results in these figures, it is useful to bear in mind that an eastward phase propagation of a given variable is characterized by a westward shift of the extreme at different locations in longitude with time lag, and that temporal phase differences between variables at a given location are manifested by a spatial displacement of the extreme. For example, for the eastward-propagating phenomena analyzed here, a *lead* in the temporal phase of one variable x relative to another variable y at a given location is equivalent to a westward shift of the extreme in x relative to those in y at a given time. Conversely, a *lag* in the temporal phase of one variable relative to another implies an eastward displacement in the spatial phase. Thus, temporal lags and spatial displacements

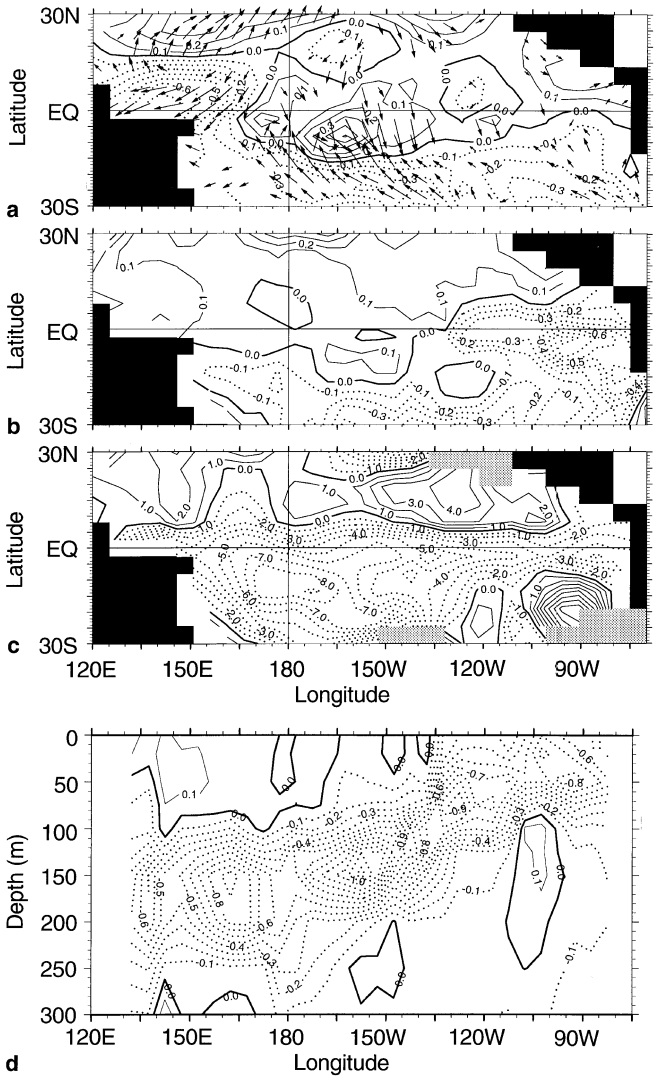

Fig. 8a–d The same as in Fig. 5 but for the reference time leading gridpoint data by one year

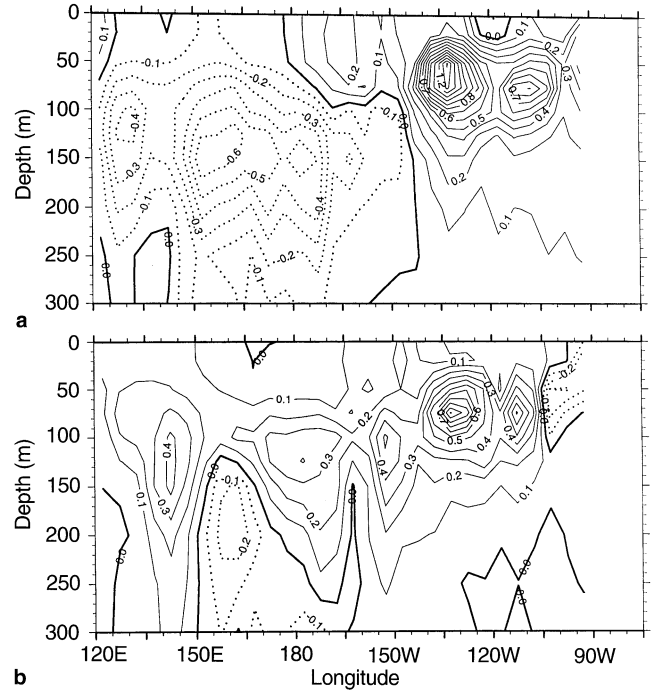

Fig. 9a, b Zonal-depth sections of the linear regression patterns along 12.5 °N with the reference time lagging temperature anomaly data by **a** 0 year, and **b** +1 year, respectively. The contour interval is 0.1 °C

can be used interchangeably for describing the phase relationships among different variables (Lau et al. 1992).

In the eastern equatorial Pacific (Fig. 11), El Nino conditions can be clearly seen at zero time lag: negative SLP and westward zonal wind anomalies, positive temperature anomalies in the upper ocean and a deepening of the 20 °C isotherm. The regression curves also indicate that fluctuations in SLP and the zonal surface winds are almost out-of-phase with those in SST, i.e., warm SST near zero lag is accompanied by large negative anomalies of SLP and zonal winds. Within the ocean, temperature variations at different depths and the 20 °C isotherm depth are approximately in-phase.

In the central equatorial Pacific (Fig. 12), El Nino conditions (near zero time lag) are characterized by negative SLP, eastward zonal wind, and positive SST anomaly extremes, but by positive anomaly extremes of temperature at 125 m depth and the 20 °C isotherm at –1 y time lag. Thus, variations in zonal wind, SST and temperature at 50 m depth are approximately in-phase, but have temporal phase differences with temperature at 125 m depth and the 20 °C isotherm depth; relative to a positive SST signal, the maximum subsurface anomalies exhibit a lead of one year (i.e., westward shift at this location). Inspection of regression curves in longitude along the equator reveals that such phase differences (or westward displacement of subsurface anomaly extreme relative to SST anomalies) prevail throughout the central equatorial Pacific. Thus, the thermocline is not in equilibrium with SST and surface winds in the central equatorial regions. In the western equatorial Pacific (figures not given), El Nino conditions with the extreme at zero time lag are manifested by eastward zonal wind, positive SLP and negative temperature anomalies in the ocean. Variations in SLP and surface zonal winds are almost in-phase; so are temperature variations in the upper ocean and the 20 °C isotherm depth. But variations in the ocean are out-of-phase with those in the atmosphere.

Examination of the regression curves indicates a phase reversal of anomaly patterns from west to east along the equator (Figs. 11–12). During an El Nino year at zero time lag, SST is warm in the central and eastern equatorial Pacific but is cold to the west; zonal surface winds are eastward in the western and central

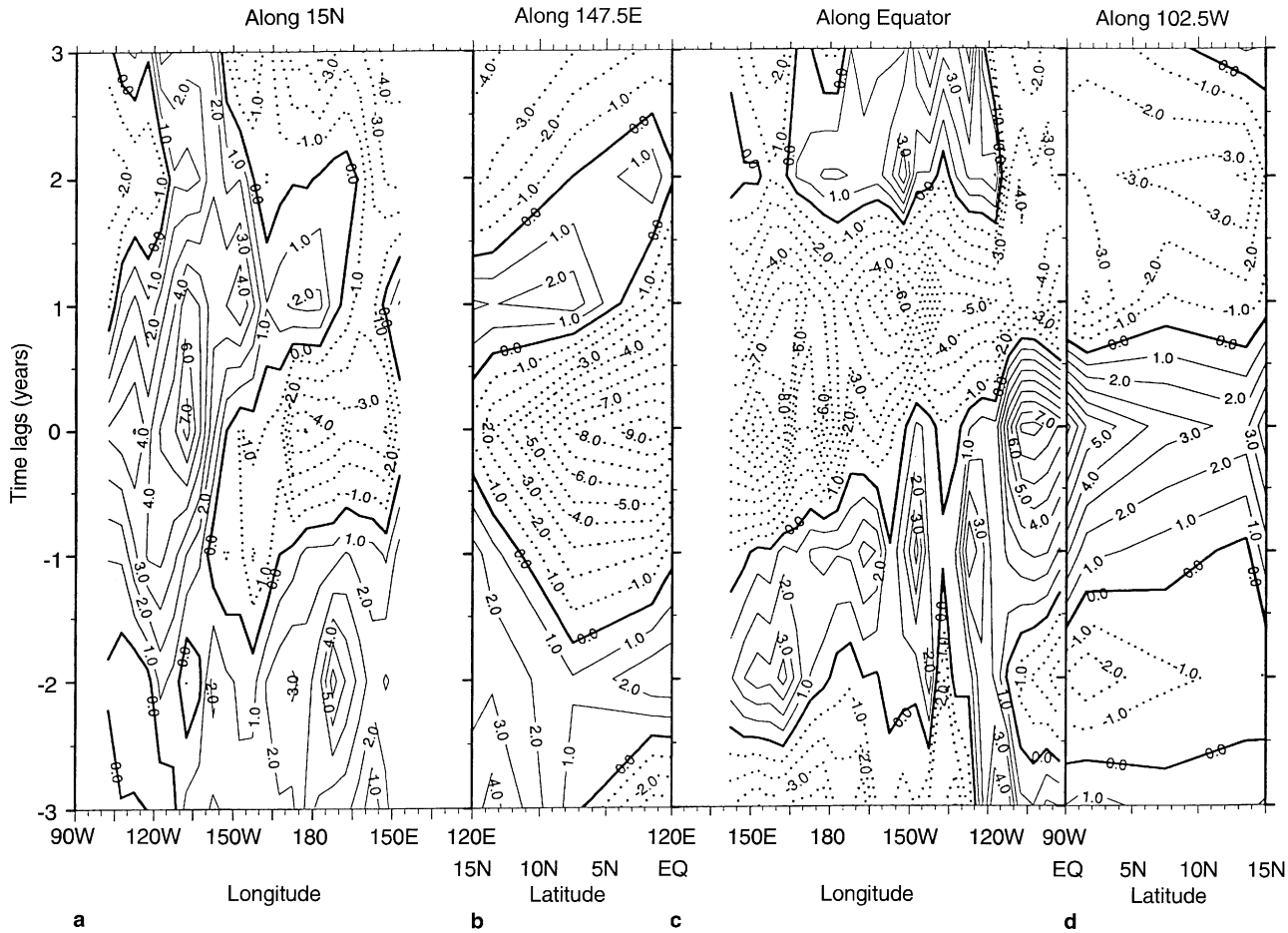

Fig. 10a–d Temporal variations in the regression coefficients of the 20 °C isotherm depth on a circuit around the northern tropical Pacific. **a** Zonal section along 15 °N; **b** meridional section along 147.5 °E; **c** zonal section along the equator; **d** Meridional section along 102.5 °W. Note the same plotting strategy as in Fig. 3. The contour interval is 1 m, with *negative* contours *dotted*

equatorial Pacific but westward to the east. In the subsurface ocean, the out-of-phase relationship is much more pronounced between fluctuations in temperature in the west and in the east. Further, these anomalies show a coherent phase relationship to one another. In the western and eastern equatorial Pacific, variations in SST are positively correlated with thermocline anomalies but are negatively correlated with zonal surface winds. In the central equatorial Pacific (Fig. 12), variations in SST and zonal surface winds are positively correlated, but have phase lags with subsurface temperature anomalies. Thus, surface conditions in the eastern equatorial Pacific can be interpreted as manifesting a delayed effect of the subsurface anomaly conditions to the west.

6 Conclusion and discussion

There are considerable differences in the characteristic phase propagation among atmospheric and oceanic anomalies on and off the equator in the tropical Pacific climate system. Variations in surface zonal winds and SSTs exhibit a standing pattern without obvious phase propagation in time. Phase propagation is, however, clearly evident at subsurface ocean depths: eastward along the equator and westward off the equator. Depending on geographic locations, there are coherent phase relations among some key anomaly fields. Surface zonal winds and SSTs fluctuate approximately in-phase in time, but have spatial phase differences. Along the equator, zonal mean thermocline depth anomalies are not in equilibrium with zonal wind stress forcing. Subsurface thermocline fluctuations are not in equilibrium with SST anomalies either. Significant spatial and temporal phase differences can be found between variations in SSTs and subsurface temperatures, with the former lagging the latter and displaced to the east along the equator. The thermocline temperature variations in the western Pacific are shown to precede those in the central and eastern equatorial upper ocean. Further, large off-equatorial anomalies are observed at subsurface depths during the El Nino evolution and

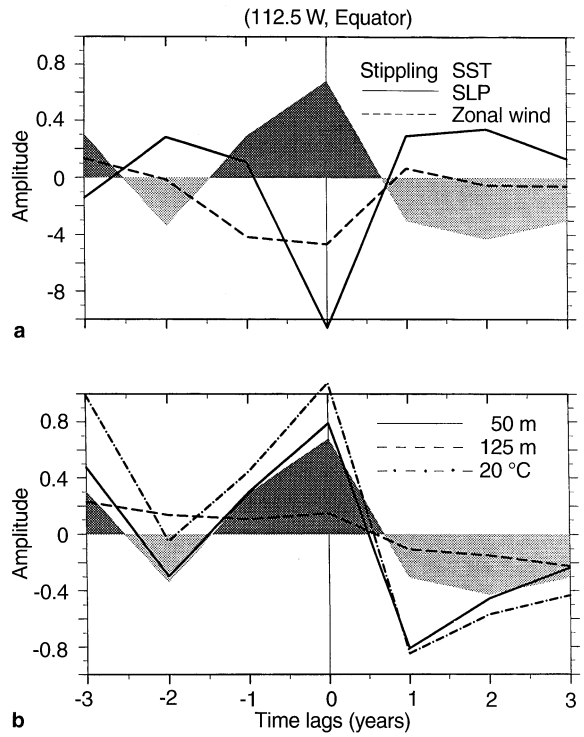

Fig. 11a, b Temporal variations in the linear regression coefficients at (112.5 °W, equator) between the reference time and SLP (*solid line*) and zonal winds (*dashed line*) in the *upper-panel*, and the 20 °C isotherm depth (dash-*dotted line*), temperature at 50 m depth (*solid line*) and 125 m depth (*dashed line*) in the *lower panel*. As an indicator of the ENSO evolution, and to serve as a common frame of reference for discussing the phase relationships, temporal variations of the SST regression coefficients are plotted both in the *upper* and *lower panels* (*stippling*). The anomalies have been scaled to about 1

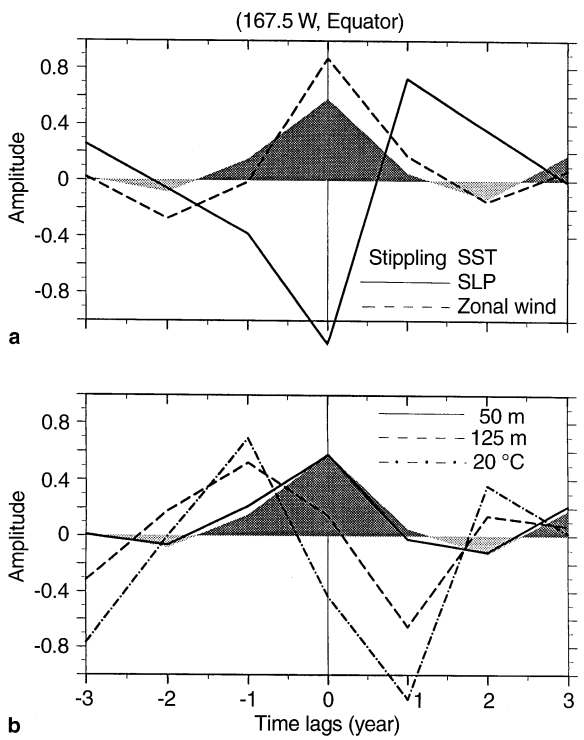

Fig. 12a, b The same as in Fig. 11 but for results at (167.5 °W, equator)

can be traced to the eastern boundary regions and further to the equator, and, thus, are not simply forced by local wind forcing alone.

The basinwide phase propagation pattern observed at subsurface depth can be understood partially as water discharge processes from the western Pacific to the east and further to high latitudes (Wyrtki 1986; Zebiak and Cane 1987; Zebiak 1989; Jin 1996, 1997), and partially by the modified delayed oscillator physics (Philander et al. 1992; Chao and Philander 1993). The apparent westward propagation signal off the equator is likely due to the oceanic Rossby wave that originates from the eastern boundaries as well as a forced response by local winds. In addition, the zonal transfer of water mass from the west to east along the equator during an El Nino development appears to involve advective processes as well (Picaut et al. 1997).

These observational results have a number of implications. The striking phase differences at the sea surface and at depth are indicative of a nonequilibrium behavior of ocean response to surface winds. If the surface winds were kept invariant in time, the ocean will continue to adjust to earlier changes in the winds. Ocean anomalies are expected to be excited by wind anomalies that prevail during periods of well-developed SST anomalies, but will freely propagate through the region or during the periods of weak wind anomalies. Further, the slow phase propagation around the basin indicates an adjustment in the subsurface ocean due to its nonequilibrium with winds on the interannual time scale. On one hand, the phase propagation of subsurface thermal anomalies can initiate SST variations in the central and eastern equatorial Pacific, which, in turn, induce wind anomalies: an unstable air-sea interaction mechanism operates in the tropics and produces large anomalies characteristic of El Nino conditions. After an El Nino event, on the other hand, the equatorial thermocline is anomalously shallow due to an off-equatorward discharge of equatorial warm water. This leaves a nonequilibrium between the zonal mean thermocline anomalies and wind stress along the equator. To achieve a new balance, ocean dynamical adjustment is in order (e.g., Zebiak and Cane 1987; Jin 1997). On the equator, eastward movement of cold subsurface anomaly initiates cold SST anomalies in the central and eastern equatorial Pacific and triggers coupled air-sea interactions, leading to La Nina development. Off the equator, the discharged warm anomalies appear to propagate westward from the eastern boundary region. This propagating warm anomaly, together with a directly forced signal by easterly wind anomalies associated with the La Nina event, may serve as the origin of the next warm event. This coherent subsurface phase propagation and its relations with variations in SSTs and surface winds (i.e., phase lag and noneqilibrium response) would permit a continual oscillation in the tropical Pacific climate system. The basinwide subsurface phase propagation

appears to intermittently initiate and terminate SST anomalies in the central and eastern equatorial Pacific on an interannual scale, thus providing a phase transition mechanism and determining the slow time scale of ENSO.

Different prototype models have been suggested for ENSO cycles. The central differences are physical processes that determine the slow time scales of ENSO and its phase transition mechanism. Based on observational analyses, Zhang and Levitus (1997) present an evaluation of current ENSO theories and model simulations, indicating that there are considerable discrepancies as compared to the corresponding observations. It appears that no single theory can currently explain all aspects of the observed ENSO evolution. More recently, Jin (1996, 1997) proposes a new conceptual model for ENSO based on the positive feedback of tropical air-sea interaction and the recharge-discharge of the equatorial heat content. Some identified key elements and processes in this new recharge oscillation mechanism are present and are more relevant to our data analyses, such as nonequilibrium between the zonal mean equatorial thermocline depth anomalies and wind stress.

Acknowledgements We thank Sydney Levitus and other staff at the Ocean Climate Laboratory (NODC/NOAA) for their help and support in analyzing the observational data. We thank Tony Busalacchi, J. Picaut, Fei-Fei Jin and two anonymous reviewers for their useful comments. This research is supported by the National Oceanic and Atmospheric Administration (NOAA) through grant NA 16RC022802 and by the NOAA Climate and Global Change Program.

References

Battisti DS, Hirst AC (1989) Interannual variability in the tropical atmosphere-ocean system: influence of the basis state, ocean geometry and nonlinearity. J Atmos Sci 46:1687–1712

Bjerknes J (1969) Atmospheric teleconnections from the equatorial Pacific. Mon Weather Rev 7:163–172

Chao Y, Philander SGH (1993) On the structure of the Southern Oscillation. J Clim 6:450–469

Da Silva M, Young CC, Levitus S (1994) Atlas of surface marine anomalies, vol 2: directly observed quantities. NOAA Atlas NESDIS 7

Hirst AC (1986) Unstable and damped equatorial modes in simple coupled ocean-atmosphere models. J Atmos Sci 43:606–630

Jin FF, Neelin JD (1993) Modes of interannual tropical ocean-atmosphere interaction-a unified view, part I: numerical results. J Atmos Sci 50:3477–3503

Jin FF (1996) Tropical ocean-atmosphere interaction, the Pacific cold tongue, and the El Nino-Southern. Oscillation. Science 274:76–78

Jin FF (1997) An equatorial ocean recharge paradigm for ENSO. Part I: conceptual model. J Atmos Sci 54:811–829

Kessler WS (1990) Observations of long Rossby waves in the Northern tropical Pacific. J Geophys Res 95:5183–5217

Kessler WS, McPhaden MJ (1995) Oceanic equatorial waves and the 1991–93 El Nino. J Clim 8:1757–1774

Latif M, Sterl A, Maier-Reimer E, Junge MM (1993) Climate variability in a coupled GCM, part I: the tropical Pacific. J Clim 6:5–21

Lau NC, Philander SGH, Nath MJ (1992) Simulation of ENSO-like phenomena with a low resolution coupled GCM of the global ocean and atmosphere. J Clim 5:284–307

Levitus S, Boyer TP, Antonov J (1994) World ocean atlas, vol 5: interannual variability of upper ocean thermal structure. NOAA Atlas NESDIS 5, US Government Printing Office, Washington, D.C.

McCreary JP, Anderson DLT (1984) A simple model of El Nino and Southern Oscillation. Mon Weather Rev 112:934–946

McWilliams JC, Gent PR (1978) Coupled air and sea model for the tropical Pacific. J Atmos Sci 35:962–989

Neelin JD (1990) A hybrid coupled general circulation model for El Nino studies. J Atmos Sci 47:674–693

Neelin JD, Latif M et al. (1992) Tropical air-sea interaction in general circulation models. Clim Dyn 7:73–104

Philander SGH, Yamagata T, Pacanowski RC (1984) Unstable air-sea interactions in the tropics. J Atmos Sci 41:603–613

Philander SGH, Lau NC, Pacanowski RC, Nath MJ (1992) Simulation of ENSO with a global atmospheric GCM coupled to a high-resolution, tropical Pacific Ocean GCM. J Clim 5:308–329

Picaut J, Masia F, du Penhoat Y (1997) An advective-reflective conceptual model for the oscillatory nature of the ENSO. Science 277:663–666

Rasmusson EM, Carpenter TH (1982) Variations in tropical sea surface temperature and surface wind stress associated with the Southern Oscillation/El Nino. Mon Weather Rev 110:354–384

Schneider EK, Huang B, Shukla J (1995) Ocean wave dynamics and El Nino. J Clim 8:2415–2439

Schopf PS, Suarez MJ (1988) Vacillations in a coupled ocean-atmosphere model. J Atmos Sci 45:549–566

White WB, He Y, Pazan SE (1989) Off-equatorial westward propagating waves in the tropical Pacific during the 1982–83 and 1986–87 ENSO events. J Phys Oceanogr 19:1397–1406

Wyrtki K (1975) El Nino-the dynamic response of the equatorial Pacific Ocean to atmospheric forcing. J Phys Oceanogr 5:572–584

Wyrtki K (1986) Water displacements in the Pacific and the genesis of El Nino cycles. J Geophys Res 91:7129–7132

Yamagata T (1985) Stability of a simple air-sea coupled model in the tropics. In: Nihoul, J.C.J. (ed) Coupled ocean-atmospheric models. Elsevier, Amsterdam, pp 637–658

Zebiak SE, Cane MA (1987) A model ENSO. Mon Weather Rev 115:2262–2278

Zebiak SE (1989) Oceanic heat content variability and El Nino cycles. J Phys Oceanogr 19:475–486

Zhang RH, Levitus S (1996) Structure and evolution of interannual variability of the tropical Pacific upper ocean temperature. J Geophys Res 101:20 501–20 524

Zhang RH, Levitus S (1997) Interannual variability of the coupled tropical Pacific ocean-atmosphere system associated with the El Nino/Southern Oscillation. J Clim, 10:1312–1330